2014 IEEE International Conference on Robotics & Automation (ICRA)
Hong Kong Convention and Exhibition Center
May 31 - June 7, 2014. Hong Kong, China

Model Based Sliding Mode Control for a 3-DOF Translational Micro Parallel Positioning Stage

Shunli Xiao and Yangmin Li*, *Senior Member, IEEE*

***Abstract*— This paper presents mechanical system dynamics modeling analysis and control of a novel compliant flexure-based micro-parallel positioning stage. The designed micro-parallel positioning stage consists of a mobile plate, a fixed base, and three limbs with identical kinematic structure. Certain geometric conditions are adopted to make the mobile plate with purely 3 translational degrees of freedoms. Each limb connects the mobile base to the fixed plate through a $\bar{P}$ (prismatic) joint and two U (universal) joints in sequence, where $\bar{P}$ joint is the active joint driven by a pair of novel electromagnetic actuators assembled on the fixed base. The prototype of the designed system is fabricated, dynamics model of the manipulator is constructed through Lagrange method and sliding mode controller is designed based on the dynamics model.**

I. Introduction

High precision and multi degree of freedoms(DOF) are extremely important in the fields of micro/nano scale manipulation such as micro-electro-mechanical system (MEMS), optical fiber alignment, biological cell manipulation, wafer stepper lithography machines and scanning probe microscope [1]-[2]. Various micro positioning stages can be classified into serial connected or parallel connected structure, or by means of actuating types such as piezoceramics (PZT), shape memory alloy (SMA) and electro active polymer actuator(EPA) etc. With different structure, the positioning stage possesses different advantages and disadvantages. For some piled like serial connected multi-DOF micro positioning stage, its kinematic models can be built easily and can be controlled conveniently, but the positioning errors may be accumulated and be amplified from the low stages to the end-effector. The accumulation of the errors will affect the precision of the serial connected manipulator seriously, even will make it impossible to obtain ultrahigh precision [3]. It is well known that parallel kinematic mechanism possesses great advantages over traditional serial robot arms, such as high rigidity, high accuracy, and high load carrying capacity, etc. [4]-[7]. In addition, the parallel manipulator is able to provide a very complicated motion for the end-effector in a flexible way with many degrees of freedom (DOF) [8]-[11]. For high resolution and accuracy required in the micro/nano manipulation field, it is almost impossible to adopt conventional mechanical parts such as sliding pairs or bearings to form ultrahigh precision manipulator. Because the very tiny friction and clearance in the conventional parts will result in larger errors to the manipulation process. However, flexure hinge-based compliant mechanical mechanisms, which realize the motion through deflections of the flexure parts, can be adopted into parallel manipulators for the manipulation of requiring ultra high precision. Therefore, the parallel robotic manipulator with compliant flexure-based parts attracts many researchers' attentions in recent years. For different actuation technologies of micro manipulators, the selection of actuators is also a hot research point in micro/nano manipulation field [8]. Although the PZT can possess a very high-precision and give large driving force output, it can only be used in some very small working range situations [12]. As for the actuator made by SMA with a large output working range, its response is slow and needs complex heating/cooling auxiliaries. Compared with the conventional PZT or SMA actuators in consideration of larger stroke, high-resolution and large output force, the electromagnetic actuator will be a better choice.

In both micro/nano scale or macro scale manipulation field, many studies focus on industrial applications which need a pure translational motion such as a motion simulator, a positioning tool in an assembly line, active vibration isolation, etc. It can be observed that, a lot of industrial robots are realized via serial structure such as famous PUMA robot. Their precisions in range of millimeters or sub-millimeters are enough for most macro manipulation [13]. As for fast response, higher resolution and complex motion requirement manipulation such as active vibration isolation, surgery robot, complex surface milling machine, etc., most these robots are realized through parallel robot such as famous DELTA robot with precision range of sub millimeter to tens of microns[6]-[7],[11]. With this trend, most high performance multi-DOFs micro manipulation are realized with parallel structure due to its advantages [14].

Since a flexure machine with notched hinges behaves the merits of the flexure-based mechanism for micro/nano manipulation in terms of vacuum compatibility, no backlash property, no non-linear friction, simple joint structure and easy to manufacture, they have been widely used for micro-precision machinery [15]-[16]. Combined with the high performance of the parallel robot, flexure parallel mechanism (FPM) possesses high flexibility and high natural frequencies, there are no error accumulations and no lubrication needed. Because of these advantages, the FPM is widely employed as the ultra-precision manipulation system in var-

This work was supported in part by National Natural Science Foundation of China (61128008), Macao Science and Technology Development Fund (108/2012/A3), Research Committee of University of Macau (MYRG183(Y1-L3)FST11-LYM, MYRG203(Y1-L4)-FST11-LYM).

S. Xiao and Y. Li are with the Department of Electromechanical Engineering, University of Macau, Av. Padre Tomás Pereira, Taipa, Macao SAR, China. *Y. Li(Corresponding author) is a visiting Chair Professor with School of Mechanical Engineering, Tianjin University of Technology, Tianjin 300384, China (e-mail: ymli@umac.mo).

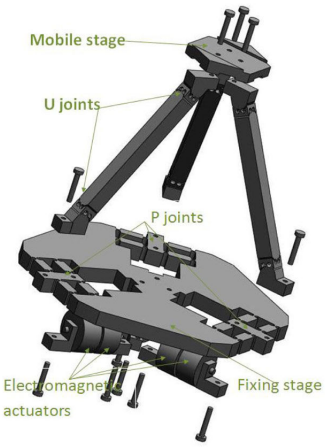

Fig. 1. 3D prototype design of the mechanical system.

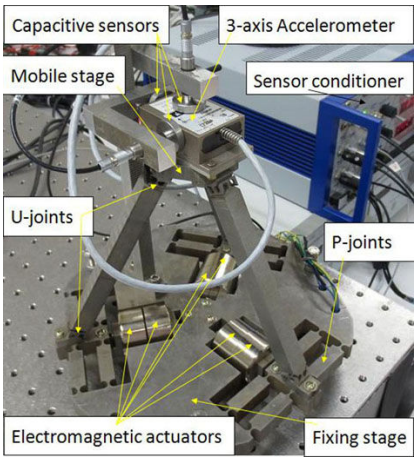

Fig. 2. Mechanical prototype of the manipulator.

ious fields such as fiber optic coupling, micro-machining, vibration isolation device, and semiconductor production.

In this paper, to design a 3-DOF purely translational moving micro/nano manipulator, the mechanism structure and the driving actuators are compared and selected carefully. Some flexure hinge-based micro parallel structures are constructed, and electromagnetic actuators are adopted to drive the designed FPM. Compared with the PZT directly actuated micro manipulator, it owns advantages in terms of larger working range, large output force and fast response [17]-[18]. Compared with the maglev micro manipulator [19], it possesses a high payload capability. Besides, the proposed electromagnetic driving 3-DOF translational micro positioning stage can be fabricated easily at very low cost. In the followings of the paper, to cope with complex coupled force and hysteresis problems, a concise dynamics modeling via Lagrange method is built and sliding mode controller is designed to control the FPM for fast response and high precision performance.

II. Architecture Description of the Manipulator

The 3-D prototype design of the positioning stage is shown in Fig.1, it is with parallel structure. The prototype and the whole experiments system can be observed in Fig.2. A mobile stage, a fixed stage, and three identical limbs are assembled in symmetry. Each limb between the fixed stage and mobile stage is connected through a $\bar{P}$ (prismatic) joint and two U (universal) joints in sequence, where $\bar{P}$ joint is the active joint with a pair of novel electromagnetic actuators on the fixed stage. Thus, the mobile platform is attached to the base through the three identical and rotational assembled limbs.

In order to realize the pure translational motion characteristics on the mobile stage with respect to the base stage, the designed mechanism should meet certain geometric conditions as shown in the Fig.3, which were deeply studied before in [5]-[6],[20]-[21].

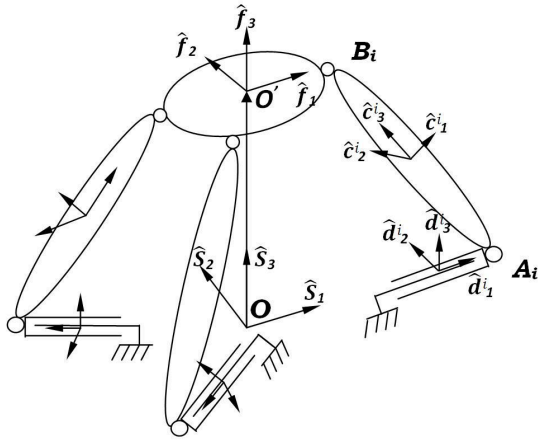

Fig. 3. The coordinate system of the 3-PUU micro parallel platform.

III. Dynamics Model of the Mechanical System

Generally, there are two methods to build the mechanical system's dynamical models. One is the vector method, another one is energy method [22]. Since the Lagrange method who belongs to the first category has distinctly advantages for complex system in general, it can obtain the simplest and most intuitive dynamics equations, it is adopted to derive the designed micro-parallel manipulator's dynamics model in this research.

A. Kinematic Analysis

1) Coordinate System: Let $\mathbf{P}=[p_1\ p_2\ p_3]^T$ be the vector of the three P-joint's length variables, let $\mathbf{L}=[l_1\ l_2\ l_3]^T$ be the vector of the three limb's length variables, $\mathbf{p}_i$ be the vector of $\overrightarrow{OA_i}$ and lie in the directions of vectors $\hat{d}^i_1$, $\mathbf{b}_i$ be the vector of $\overrightarrow{O'B_i}$ and lie in the directions of vectors $\hat{d}^i_1$. As shown in Fig.3, let the vector $\mathbf{r}_{OO'}=[x\ y\ z]^T$ be the vector of reference point O to the central position of the mobile stage O'. The mass of the moving stage is M and the mass of each limb is m_l. The mass of each P-joint's supporting limb and central limb is m_s and m_p, respectively. A coordinate system C_{li} (i=1, 2, 3) can be attached at the mass center of the ith limb.

The axis directions of the coordinate system are determined by the orthogonal unit vectors $\widehat{\mathbf{c}}_j^i$ (j=1,2,3). The hat on the vector indicates that it is unit length, the index i with respect to the ith limb, and the index j refers to the three vectors of the coordinate system. $\widehat{\mathbf{c}}_3^i$ is at the center of the ith limb, towards the center of the ith flexure hinge which connects the moving stage. $\widehat{\mathbf{c}}_2^i$ is perpendicular with the vector $\overrightarrow{oB_i}$ and $\overrightarrow{OA_i}$ when the moving stage is at its initial position, and $\widehat{\mathbf{c}}_1^i$ is in the direction perpendicular with both $\widehat{\mathbf{c}}_2^i$*and*$\widehat{\mathbf{c}}_3^i$. Let a P-joint's central beam be fixed with a right-handed coordinate system D_i (i=1,$\cdots$,3) and it is located at the mass center of the ith P-joint's beam, the axis directions are determined by the unit vectors $\widehat{\mathbf{d}}_j^i$ (j=1,$\cdots$,3) who are perpendicular with each other. Among them, $\widehat{\mathbf{d}}_1^i$ is along ith limb, towards the ith flexure hinge which connects the limb. $\widehat{\mathbf{d}}_2^i$ is perpendicular with the plane A_iOO' when the moving stage is at its initial position, and $\widehat{\mathbf{d}}_3^i$ is in the direction perpendicular with both $\widehat{\mathbf{d}}_2^i$ and $\widehat{\mathbf{d}}_3^i$. Define a reference coordinate system $\widehat{\mathbf{s}}_j$ on the fixed stage at the center O with the vector $\widehat{\mathbf{s}}_1$ towards to the point A_1 and $\widehat{\mathbf{s}}_3$ vertical to the fixed stage. Attach a frame $\widehat{\mathbf{f}}_j$ to the moving stage at the center o' with $\widehat{\mathbf{f}}_1$ towards the point B_1 and $\widehat{\mathbf{f}}_3$ vertical to the moving stage. $\Re$ is a transformation matrix from $\widehat{\mathbf{f}}_j$ coordinate system to $\widehat{\mathbf{s}}_j$. $\Re_{ci}$ is the transformation matrix from $\widehat{\mathbf{c}}_j$ coordinate system to $\widehat{\mathbf{s}}_j$. In order to calculate the rotational angles of the flexure hinges, an initial frame is attached on the initial C_i^* with axis directions forward to the frame set of unit vectors $\widehat{\mathbf{c}}_{j0}^i$ when the moving stage is at the initial position. The directions of the axis are determined by frames $\widehat{\mathbf{c}}_j^i$ on the limbs when the mobile stage is at the initial position.

The rotational matrix of the frame $\widehat{\mathbf{c}}_j^i$ is with respect to $\widehat{\mathbf{c}}_{j0}^i$, which can be described with the rotational angles q_1^i about the axes $\widehat{\mathbf{c}}_{10}^i$ and q_2^i about the axes $\widehat{\mathbf{c}}_{20}^i$. It can be denoted as $\Re_{ci0}$, that is:

$$\Re_{ci0} = \begin{bmatrix} \widehat{\mathbf{c}}_{10}^i & \widehat{\mathbf{c}}_{20}^i & \widehat{\mathbf{c}}_{30}^i \end{bmatrix}^{-1} \begin{bmatrix} \widehat{\mathbf{c}}_1^i & \widehat{\mathbf{c}}_2^i & \widehat{\mathbf{c}}_3^i \end{bmatrix} \tag{1}$$

.

Since the sine value of small-angles can be approximated as the angles q_k^i, the rotation matrix can be rewritten as:

$$\Re_{ci0} = \begin{bmatrix} 1 & 0 & q_2^i \\ 0 & 1 & -q_1^i \\ -q_2^i & q_1^i & 1 \end{bmatrix} \tag{2}$$

.

2) Generalized Speeds and Accelerations of the System: Let $\mathbf{v}_{o'}$ be the generalized speeds of the system as the time derivation of the generalized parameters of $\mathbf{v}_{o'}$=$[x\ y\ z]^T$ in the inertial reference frame:

$$\mathbf{v}_{o'} = \begin{bmatrix} \dot{x} & \dot{y} & \dot{z} \end{bmatrix}^T \tag{3}$$

.

Let $\underline{\omega}_{C_i^*}$ be the angular velocity of each limb to the initial limb position. The position vectors are:

$$\begin{aligned} \mathbf{r}_{oo'} &= l_i\widehat{\mathbf{c}}_3^i + \mathbf{p}_i - \mathbf{b}_i \\ \mathbf{r}_{m_i} &= l_i\widehat{\mathbf{c}}_3^i + \mathbf{p}_i \\ \mathbf{r}_{C_i^*} &= \frac{l_i}{2}\widehat{\mathbf{c}}_3^i + \mathbf{p}_i \end{aligned} \tag{4}$$

Differentiating Eq. 4 with respect to time:

$$\begin{aligned} \mathbf{v}_{o'} &= \dot{\mathbf{p}}_i + l_i\underline{\omega}_{C_i^*} \times \widehat{\mathbf{c}}_3^i \\ \mathbf{v}_{m_i} &= \mathbf{v}_{o'} \\ \mathbf{v}_{C_i^*} &= \frac{\dot{\mathbf{p}}_i + l_i\underline{\omega}_{C_i^*} \times \widehat{\mathbf{c}}_3^i}{2} = \frac{\mathbf{v}_{o'}}{2}. \end{aligned} \tag{5}$$

From Eq.5, it can be derived by

$$\dot{\mathbf{p}}_i = \mathbf{v}_{o'} - l_i\underline{\omega}_{C_i^*} \times \widehat{\mathbf{c}}_3^i \tag{6}$$

and:

$$\underline{\omega}_{C_i^*} = \frac{\widehat{\mathbf{c}}_3^i \times (\mathbf{v}_{o'} - \dot{\mathbf{p}}_i)}{l_i} \tag{7}$$

Then, the linearized accelerations can be derived by

$$\begin{aligned} \mathbf{a}_{o'} &= l_i\underline{\varepsilon}_{C_i^*} \times \widehat{\mathbf{c}}_3^i + l_i\underline{\omega}_{C_i^*} \times (\underline{\omega}_{C_i^*} \times \widehat{\mathbf{c}}_3^i) + \ddot{\mathbf{p}}_i \\ \mathbf{a}_{C_i^*} &= \frac{\mathbf{a}_{o'}}{2} \end{aligned} \tag{8}$$

From Eq. 8, cross-multiplying both sides by $\widehat{\mathbf{c}}_3^i$, we can have

$$\underline{\varepsilon}_{C_i^*} = \frac{\widehat{\mathbf{c}}_3^i \times \mathbf{a}_{o'} - l_i(\underline{\omega}_{C_i^*} \cdot \widehat{\mathbf{c}}_3^i)(\underline{\omega}_{C_i^*} \times \widehat{\mathbf{c}}_3^i) - \widehat{\mathbf{c}}_3^i \times \mathbf{p}_i}{l_i} \tag{9}$$

where the $\underline{\varepsilon}_{C_i^*}$ is the angular acceleration of each limb.

B. Dynamics Model via Lagrange Method

In this research, the dynamics model is established through Lagrange's equation which is a well known tool for establishing equations of dynamics systems. The key point of the Lagrange's equations is to find out the kinematic energy and potential energy of the system, which can be formulated through the relationships of the moving coordinate system and the initial coordinate system as presented in the previous subsection.

1) Kinematic Energy of the System: For the moving stage, the kinetic energy can be derived by

$$E_{kM} = \frac{1}{2}M(\dot{x}^2 + \dot{y}^2 + \dot{z}^2) \tag{10}$$

For each limb, assume rotations about a fixed axis, the kinetic energy can be given by

$$E_{kl_i} = \frac{1}{2}m_l\|\mathbf{v}_{C_i^*}\|^2 + \frac{1}{2}I_{C_i}\underline{\omega}_{C_i^*}^2 \tag{11}$$

where

$$I_{C_i} = \frac{1}{3}m_l l_i^2$$

For each P-joint with electromagnetic actuators in the base plane:

$$E_{kp_i} = \frac{1}{2}m_p\dot{\mathbf{p}}_i^2 + \frac{1}{2}m_{pl}(\frac{\dot{\mathbf{p}}_i}{2})^2 \tag{12}$$

where m_p is the mass of the P limb including the electromagnetic actuators, while m_{pl} is the mass of the four sub-limb in the P-joint.

According to Eq. 12, the kinetic energy of the whole system can be derived by

$$\begin{aligned} E_k &= E_{kM} + \sum_{i=1}^{3} E_{kl_i} + \sum_{i=1}^{3} E_{kp_i} \\ &= \frac{1}{2}M(\dot{x}^2+\dot{y}^2+\dot{z}^2) + \sum_{i=1}^{3}(\frac{1}{2}m_l\|\mathbf{v}_{C_i^*}\|^2 \\ &+ \frac{1}{2}I_{C_i}((\dot{q}_1^i)^2+(\dot{q}_2^i)^2)) + \sum_{i=1}^{3}(\frac{1}{2}m_p\dot{\mathbf{p}}_i^2 + \frac{1}{2}m_{pl}(\frac{\dot{\mathbf{p}}_i}{2})^2) \\ &= (\frac{1}{2}M+\frac{3}{8}m_l)(\dot{x}^2+\dot{y}^2+\dot{z}^2) \\ &+ \sum_{i=1}^{3}\frac{1}{6}m_l l_i^2((\dot{q}_1^i)^2+(\dot{q}_2^i)^2)) + \sum_{i=1}^{3}(\frac{1}{2}m_p+\frac{1}{8}m_{pl})\dot{\mathbf{p}}_i^2 \end{aligned} \tag{13}$$

2) Potential Energy of the System: The potential energy of moving platform is given by

$$E_{pM} = Mgz \tag{14}$$

Since the system is investigated in micro-motion environment, according to the Eq. 9, we can obtain

$$\widehat{\mathbf{c}}_3^i = \frac{1}{l_i}\begin{bmatrix} x-x_{A_i}+x_{B_i} \\ y-y_{A_i}+y_{B_i} \\ z-z_{A_i}+z_{B_i} \end{bmatrix} \tag{15}$$

Let

$$\begin{bmatrix} \widehat{\mathbf{c}}_{10}^i & \widehat{\mathbf{c}}_{20}^i & \widehat{\mathbf{c}}_{30}^i \end{bmatrix}^{-1} = \begin{bmatrix} r_{11}^i & r_{12}^i & r_{13}^i \\ r_{21}^i & r_{22}^i & r_{23}^i \\ r_{31}^i & r_{32}^i & r_{33}^i \end{bmatrix} \tag{16}$$

According to Eq. (15) and (16), the consecutive positive rotations q_1^i and q_2^i about the moved two-axis are:

$$\frac{1}{l_i}\begin{bmatrix} r_{11}^i & r_{12}^i & r_{13}^i \\ r_{21}^i & r_{22}^i & r_{23}^i \\ r_{31}^i & r_{32}^i & r_{33}^i \end{bmatrix}\begin{bmatrix} x-x_{A_i}+x_{B_i} \\ y-y_{A_i}+y_{B_i} \\ z-z_{A_i}+z_{B_i} \end{bmatrix} = \begin{bmatrix} q_2^i \\ -q_1^i \\ 1 \end{bmatrix}$$

$$q_1^i = H_{1i} - \frac{r_{21}^i}{l_i}x - \frac{r_{22}^i}{l_i}y - \frac{r_{23}^i}{l_i}z \tag{17}$$

$$q_2^i = H_{2i} + \frac{r_{11}^i}{l_i}x + \frac{r_{12}^i}{l_i}y + \frac{r_{13}^i}{l_i}z$$

where

$$H_{1i} = \frac{r_{21}^i}{l_i}(x_{A_i}-x_{B_i}) + \frac{r_{22}^i}{l_i}(y_{A_i}-y_{B_i}) + \frac{r_{23}^i}{l_i}(z_{A_i}-z_{B_i})$$

$$H_{2i} = \frac{r_{11}^i}{l_i}(x_{B_i}-x_{A_i}) + \frac{r_{12}^i}{l_i}(y_{B_i}-y_{A_i}) + \frac{r_{13}^i}{l_i}(z_{B_i}-z_{A_i})$$

For each limb, the potential energy can be written as:

$$E_{pl_i} = m_l g\frac{z-z_{A_i}+z_{B_i}}{2} + k_1^i(q_1^i)^2 + k_2^i(q_2^i)^2 \tag{18}$$

For each P-joint, the potential energy can be derived as:

$$E_{pp_i} = k_3^i(q_3^i)^2 \tag{19}$$

where $q_3^i = \frac{\|\mathbf{p}_i\|-p_{10}}{l_{pli}}$, p_{10} is $\|\mathbf{p}_i\|, (i=1)$, at the initial position, and l_{pli} is the length of the sub-limb in the P-joint.

Hence, the potential energy of the whole system can be given by

$$\begin{aligned} E_p = Mgz + \\ \sum_{i=1}^{3}(m_l g\frac{z-z_{A_i}+z_{B_i}}{2} + k_1^i(q_1^i)^2 + k_2^i(q_2^i)^2 + k_3^i(q_3^i)^2) \end{aligned} \tag{20}$$

3) Lagrange's Equations: Let $F_j^{a_i}$ be the actuated force of each limb associated to the limb-j respectively. The Lagrange's equations are:

$$\frac{d}{dt}(\frac{\partial E_k}{\partial u_j}) - \frac{\partial E_k}{\partial q_j} + \frac{\partial E_p}{\partial q_j} = \sum_{i=1}^{3} F_j^{a_i} \tag{21}$$

From above equation, the final forward dynamics equation of this parallel multi-body system can be written as:

$$\mathbf{M}\cdot\ddot{\mathbf{q}} + \mathbf{K}\cdot\mathbf{q} = \mathbf{Q}_F + \boldsymbol{f}_D \tag{22}$$

where $\mathbf{M}$, $\mathbf{K}$ and $\mathbf{Q}_F$ can be derived from the Eq.21

$$\mathbf{Q}_F = \sum_{i=1}^{3} F^{a_i} + \mathbf{Q}_L \tag{23}$$

where $F_a = [F_1, F_2, F_3]^T$ is the force vector of the electromagnetic actuators generated, $F^{a_i} = F_i\hat{c}_3^i, (i=1,2,3)$ is the driving force vector of the electromagnetic actuators, and $\mathbf{Q}_L = [Q_1, Q_2, Q_3]^T$ is the force error vector through the dynamics model, $\boldsymbol{f}_D$ is the disturbance forces.

IV. Terminal Sliding-Mode Controller Design

Since the sliding mode controller shows great robust ability in handling some nonlinear or parameters unknown systems, it is an ideal controller to control the electromagnetic actuated micromanipulator [14]. But, compared with normal linear hyperplane based sliding mode, terminal sliding mode controller possesses some superior advantages such as fast, convergent in finite time, etc.. This controller is particularly useful for high precision control as it speeds up the rate of convergence near an equilibrium point [24]. Since the dynamics model of the stage is built through Lagrange method, a multi-input and multi-output terminal sliding mode controller is adopted here to control the stage. Then, let $\boldsymbol{x}_1 = \mathbf{q}$, $\boldsymbol{x}_2 = \dot{\mathbf{q}}$, $\boldsymbol{x}_3 = \ddot{\mathbf{q}}$ and $\mathbf{X} = [\boldsymbol{x}_1^T, \boldsymbol{x}_2^T, \boldsymbol{x}_3^T]^T$.

From the dynamics equation of the stage, we can assume that the external disturbance forces $\boldsymbol{f}_D$ and the uncertain dynamics parameters included in $\mathbf{Q}_L$ are bounded. Then we have $||\mathbf{Q}_L|| < \mathbf{Q}_D$ and $||\boldsymbol{f}_D|| < \mathbf{F}_D$. $\mathbf{Q}_D$ and $\mathbf{F}_D$ are positive real numbers.

Define the expected trajectory as: $\mathbf{X}_d = [\boldsymbol{x}_{1d}^T, \boldsymbol{x}_{2d}^T, \boldsymbol{x}_{3d}^T]^T = [\boldsymbol{x}_{1d}^T, \dot{\boldsymbol{x}}_{1d}^T, \ddot{\boldsymbol{x}}_{1d}^T]^T$. Then the tracking error can be : $\mathbf{E} = \mathbf{X} - \mathbf{X}_d = [\boldsymbol{e}^T, \dot{\boldsymbol{e}}^T, \ddot{\boldsymbol{e}}^T]^T$, where $\boldsymbol{e} = \boldsymbol{x}_1 - \boldsymbol{x}_{1d} = [\boldsymbol{e}_1, \boldsymbol{e}_2, \boldsymbol{e}_3]^T$.

After the tracking error is defined, the sliding surface equation can be designed as:

$$\sigma(\mathbf{X}, t) = \boldsymbol{C}\boldsymbol{E} - \boldsymbol{W}(t) \tag{24}$$

where $\boldsymbol{C} = [\boldsymbol{C}_1, \boldsymbol{C}_2, \boldsymbol{C}_3]$, $\boldsymbol{C}_i = [c_{i1}, c_{i2}, c_{i3}]$, $c_{ij}(i, j = 1, 2, 3)$ are positive real numbers, $\boldsymbol{W}(t) = \boldsymbol{C}\boldsymbol{P}(t)$. $\boldsymbol{P}(t)$ is an auxiliary matrix which is used to promise that the controller converges to equilibrium point within limited time $[0, T]$.

Following assumptions and equations are to calculate the parameters of $\boldsymbol{P}(t)$. Set $\boldsymbol{P}(t) = [\boldsymbol{p}(t)^T, \dot{\boldsymbol{p}}(t)^T, \ddot{\boldsymbol{p}}(t)^T]^T$. $\boldsymbol{p}(t) = [p_1(t), p_2(t), p_3(t)]^T$ and assume $p_i(t)$:$\mathbf{R}_+ \to \mathbf{R}$. For any positive constant $T > 0$, $p_i(t)$ is bounded in period of $[0, T]$, and $p_i(0) = e_i(0), \dot{p}_i(0) = \dot{e}_i(0), \ddot{p}_i(0) = \ddot{e}_i(0).(i = 1, 2, 3)$. The function of $p_i(t)$ can be selected as:

$$p_i(t) = \begin{cases} \sum_{k=1}^{n} \frac{1}{k!} e_i(0)^{(k)} t^k + \sum_{j=0}^{n} \left(\sum_{l=0}^{n} \frac{a_{jl}}{T^{j-l+n+1}} e_i(0)^{(l)} \cdot t^{j+n+1} \right) & 0 \le t \le T \\ 0 & t > T \end{cases} \tag{25}$$

where $n = 3$ and parameters $a_{jl}, (j, l = 0, 1, 2, 3)$ can be obtained based on the previous assumption.

After the sliding surface is designed, the terminal sliding mode control scheme can be designed as:
$F_a = -[\hat{c}_3^{1T}, \hat{c}_3^{2T}, \hat{c}_3^{3T}]^{T-1} [-M^{-1}\mathbf{K} \cdot \mathbf{q} - x_{1d}^{(3)} - p^{(3)}(t) + C_3^{-1} C_1 [\dot{\boldsymbol{e}} - \dot{\boldsymbol{p}}(t)] + C_3^{-1} C_2 [\ddot{\boldsymbol{e}} - \ddot{\boldsymbol{p}}(t)]] - [\hat{c}_3^{1T}, \hat{c}_3^{2T}, \hat{c}_3^{3T}]^{T-1} \frac{C_3^T \sigma}{\|C_3^T \sigma\|} \{\mathbf{Q}_D + \mathbf{F}_D + \Gamma\}$
where Γ is a positive real number.
To prove the stability performance of the controller, the constructed Lyapunov function can be constructed as:

$$V = \frac{1}{2} \sigma^T \sigma \tag{26}$$

Differentiating $\sigma(\mathbf{X}, t)$ with respect to time, we have
$\dot{\boldsymbol{\sigma}}(\mathbf{X}, t) = \boldsymbol{C}\dot{\boldsymbol{E}} - \boldsymbol{C}\dot{\boldsymbol{P}}(t)$
$= \boldsymbol{C} \cdot [\dot{\boldsymbol{e}}^T, \ddot{\boldsymbol{e}}^T, \boldsymbol{e}^{(3)T}]^T - \boldsymbol{C} \cdot [\dot{\boldsymbol{p}}(t)^T, \ddot{\boldsymbol{p}}(t)^T, \boldsymbol{p}^{(3)}(t)^T]^T$
$= \boldsymbol{C}_1 [\dot{\boldsymbol{e}} - \dot{\boldsymbol{p}}(t)] + \boldsymbol{C}_2 [\ddot{\boldsymbol{e}} - \ddot{\boldsymbol{p}}(t)] + \boldsymbol{C}_3 [\boldsymbol{e}^{(3)} - \boldsymbol{p}^{(3)}(t)]$
$= \boldsymbol{C}_3 [\boldsymbol{x}_1^{(3)} - \boldsymbol{x}_{1d}^{(3)} - \boldsymbol{p}^{(3)}(t)] + \boldsymbol{C}_1 [\dot{\boldsymbol{e}} - \dot{\boldsymbol{p}}(t)] + \boldsymbol{C}_2 [\ddot{\boldsymbol{e}} - \ddot{\boldsymbol{p}}(t)]$
$= \boldsymbol{C}_3 [\dot{\boldsymbol{x}}_3 - \boldsymbol{x}_{1d}^{(3)} - \boldsymbol{p}^{(3)}(t)] + \boldsymbol{C}_1 [\dot{\boldsymbol{e}} - \dot{\boldsymbol{p}}(t)] + \boldsymbol{C}_2 [\ddot{\boldsymbol{e}} - \ddot{\boldsymbol{p}}(t)]$
that is:
$\dot{\boldsymbol{\sigma}}(\boldsymbol{X}, t) = C_3 [M^{-1}\mathbf{Q}_F + M^{-1}\boldsymbol{f}_D - M^{-1}\mathbf{K} \cdot \mathbf{q} - x_{1d}^{(3)} - p^{(3)}(t)] + C_1 [\dot{\boldsymbol{e}} - \dot{\boldsymbol{p}}(t)] + C_2 [\ddot{\boldsymbol{e}} - \ddot{\boldsymbol{p}}(t)]$

Differentiating Eq.26 with respect to time, we have
$\dot{V} = \sigma^T \dot{\sigma}$
$= \sigma^T C_3 \{M^{-1}\mathbf{K} \cdot \mathbf{q} - x_{1d}^{(3)} - p^{(3)}(t) + C_3^{-1} C_1 [\dot{\boldsymbol{e}} - \dot{\boldsymbol{p}}(t)] + C_3^{-1} C_2 [\ddot{\boldsymbol{e}} - \ddot{\boldsymbol{p}}(t)] \} + \sigma^T C_3 [\hat{c}_3^{1T}, \hat{c}_3^{2T}, \hat{c}_3^{3T}]^T F_a + \sigma^T C_3 (\mathbf{Q}_L + \mathbf{f}_D)$
$\le \sigma^T C_3 \{-M^{-1}\mathbf{K} \cdot \mathbf{q} - x_{1d}^{(3)} - p^{(3)}(t) + C_3^{-1} C_1 [\dot{\boldsymbol{e}} - \dot{\boldsymbol{p}}(t)] + C_3^{-1} C_2 [\ddot{\boldsymbol{e}} - \ddot{\boldsymbol{p}}(t)] + \sigma^T C_3 [\hat{c}_3^{1T}, \hat{c}_3^{2T}, \hat{c}_3^{3T}]^T F_a + \|\sigma^T C_3\| \|(\mathbf{Q}_L + f_D)\|$

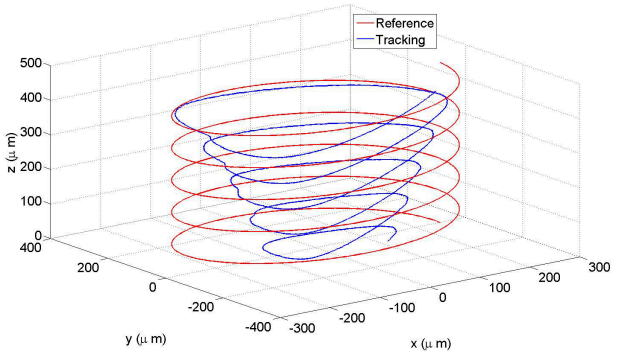

Fig. 4. Open loop helix contour tracking performance.

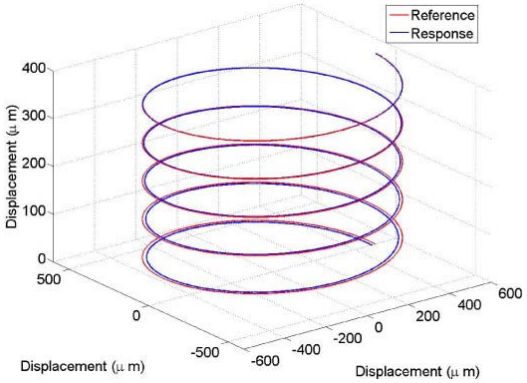

Fig. 5. Lagrange model based SMC control performance when tracking helix contour.

Substituting the control scheme F_a into $\dot{V}$, we have :
$\dot{V} \le \|C_3^T \sigma\| \, \|\mathbf{Q}_L + \boldsymbol{f}_D\| - \frac{\sigma^T C_3 C_3^T \sigma}{\|C_3^T \sigma\|} \{\mathbf{Q}_D + \mathbf{F}_D + \Gamma\}$

Since $C_3^T \sigma \sigma^T C_3 = \|C_3^T \sigma\|^2$, we have

$\dot{V} \le \|C_3^T \sigma [(\|\mathbf{Q}_L\| - \mathbf{Q}_D) + (\|\boldsymbol{f}_D\| - \mathbf{F}_D)] - \Gamma \|C_3^T \sigma\|$
$\le -\Gamma \|C_3^T \sigma\|$
$< 0 \ (\sigma \ne 0)$

Therefore, it can be concluded that the terminal sliding mode controller guarantees the asymptotic convergence of the states $\boldsymbol{x}_1$, $\boldsymbol{x}_2$, and $\boldsymbol{x}_3$ to their desired values within time $[0, T]$.

A helix trajectory is selected to assess the 3-D contouring performance of the designed 3-PUU large displacement micro-parallel manipulator as shown in Fig.4. First, the three input signals for electro-magnetic actuators are calculated by kinematics if the output of moving platform is a helix curve with a radius of 500 μm and a height of 400μm. It can be observed from the Fig.4 that the open loop contouring trajectory shows great distorted 3-D curves compared with the regular reference 3-D curves. It can be observed clearly that the outputs of the electromagnetic actuators are with

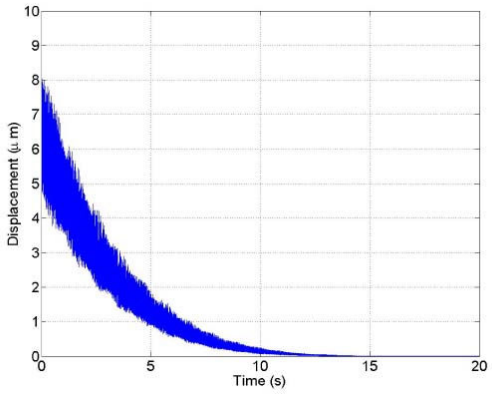

Fig. 6. Closed-loop tracking error.

both serious hysteresis and nonlinear problems which make the trajectory of the moving platform look like distortion. The maximal tracking error of the open-loop test can reach as large as 124 μm.

Therefore, a dynamics robust controller is urgently needed for manipulator. As designed in previous dynamics model and terminal sliding mode controller, it can be constructed rapidly in MATLAB/Simulink realtime environment for dSPACE system. With selected constant time parameter T as $10s$, the contouring tracking performance can be shown in Fig.5. It can be seen that the contouring performance is improved greatly compared with the previous open loop contouring experiments. The convergent process also can be shown clearly in Fig.6. The tracking error converged to zero rapidly and the tracking error decreased rapidly to 0.2 μm in the first 10 seconds, finally, the maximum tracking error can be further improved and can reach 0.02 μm within the following 10 seconds. From above experimental studies, it can be seen that the performance of the dynamics model and the designed terminal sliding mode controller are well proved. The advantages of the electromagnetic actuators driven system lie in that it can reach a large working range and a fast operation velocity, which are hard for other actuators driven system to obtain.

V. Conclusion

A novel flexure-based 3-DOF micro-positioning stage driven by electromagnetic actuators is modeled and the model based sliding mode controller is designed. The stage is featured with mainly translational mobility characteristics, simple symmetrical structure, and large motion range. For assessing the open loop contouring tracking performance, Lagrange dynamics model and terminal sliding mode controller are designed and tested on the prototype. The tracking error can be decreased rapidly to 0.2 μm within limited time. Since high resolution capacitive displacement sensors are used, the designed manipulator can be taken as a high accurate positioning stage for bio-engineering or micro-assembly application as well as micro-parallel active vibration isolation system.

References

[1] X. Zhang, C. Leung, Z. Lu, N. Esfandiari, R.F. Casper and Y. Sun, "Controlled aspiration and positioning of biological cells in a micropipette," IEEE Trans. Biomed. Eng., vol. 59, no. 4, pp. 1032-1040, 2012.

[2] Y. Zhang, X. Liu, C. Ru, Y. Zhang, L. Dong and Y. Sun, "Piezoresistivity characterization of synthetic silicon nanowires using a MEMS device," IEEE/ASME J. Microelectromech. Syst., vol. 20, no. 4, pp. 959-967, 2012.

[3] Y. Li, "Hybrid control approach to peg-in-hole problem", IEEE Robot. Auto. Mag., vol.4, no.2, pp.52-60.

[4] H. Liu, T. Huang and D. Chetwynd, "A method to formulate a dimensionally homogeneous Jacobian of parallel manipulators," IEEE Trans. Robotics, vol.27, no.1, pp.150-156, 2011.

[5] L. W. Tsai, "Systematic enumeration of parallel manipulators," Technical Research Report, 1998, No. TR 1998-33.

[6] R. Di Gregorio and V. Parenti-Castelli, "A translational 3-DOF parallel manipulator," in: J.Lenarcic, M.L.Husty(Eds.), Advances in Robot Kinematics: Analysis and Control. Kluwer, 1998, pp.49-58.

[7] Y. Yu, Z. Du, J. Yang and Y. Li, "An experimental study on the dynamics of a 3-RRR flexible parallel robot," IEEE Trans. Robotics, vol.27, no.5, pp.992-997, 2011.

[8] R. Di Gregorio, "Statics and singularity loci of the 3-UPU wrist", IEEE Trans. Robotics, vol. 20, no. 4, pp. 630-635, 2004.

[9] Y. Li and S. Staicu, "Inverse dynamics of a 3-PRC parallel kinematic machine," Nonlinear Dynamics, vol.67, no.2, pp. 1031-1041, 2012.

[10] Z. Huang and Q. C. Li, "General methodology for type synthesis of lower-mobility symmetrical parallel manipulators and several novel manipulators," Int. J. Rob. Research, vol. 21, no. 2, pp. 131-146, 2002.

[11] Y. Yun and Y. Li, "A general dynamics and control model of a class of multi-DOF manipulators for active vibration control," Mecha. Mach. Theory, vol.46, no.10, pp.1549-1574, 2011.

[12] Y. Li, J. Huang and H. Tang, "A compliant parallel XY micro-motion stage with complete kinematic decoupling," IEEE Trans. Auto. Sci. Eng., vol.9, no.3, pp.538-553, 2012.

[13] Y. Yun and Y. Li, "Modeling and control analysis of a 3-PUPU dual compliant parallel manipulator for micro positioning and active vibration isolation", Journal of Dynamic System, Measurement, and Control, Transactions of ASME, vol.134, no.2, 021001-1-9, 2012.

[14] S. Xiao and Y. Li, "Optimal design, fabrication and control of an XY micro-positioning stage driven by electromagnetic actuators," IEEE Trans. Industrial Electronics, vol.60, no.10, pp.4613-4626, 2013.

[15] Y. Yun and Y. Li, "Design and analysis of a novel 6-DOF redundant actuated parallel robot with compliant hinges for high precision positioning", Nonlinear Dynamics, vol.61, no.4, pp.829-845, 2010.

[16] S. Xiao and Y. Li, "Mobility and kinematic analysis of a novel dexterous micro gripper", IEEE Int. Conf. Robot. Auto., May 14-18, 2012, S. Paul, Minnesota, USA, pp.2523-2528.

[17] M.P. Kummer, J. Abbott, B. Kratochvil, R. Borer, A. Sengül and B. Nelson, "OctoMag: an electromagnetic system for 5-DOF wireless micromanipulation", IEEE Trans. Robotics, vol.26, no.6, pp.1006-1017, 2010.

[18] W. H. Hayt, Jr. and J. A. Buck, "Engineering electromagnetics", Sixth Edition, New York, 2001.

[19] Z. Zhang and C. Menq, "Six-axis magnetic levitation and motion control", IEEE Trans. Robotics, vol.23, no. 2, pp.196-205, 2007.

[20] D. Kim and W. K. Chung, "Kinematic condition analysis of three-DOF pure translational parallel manipulators," ASME J. Mech. Des., vol. 125, pp. 323-331, 2003.

[21] L. W. Tsai, "Kinematics of a three-DOF platform with three extensible limbs", in: J. Lenarcic, V.Parenti-Castelli(Eds.), Recent Advances in Robot Kinematics, Kluwer, 1996, pp. 401-410.

[22] L.W. Tsai, "Solving the inverse dynamics of a stewart-gough manipulator by the principle of virtual work," ASME J. Mech. Des., vol.122, pp.1-8, 2000.

[23] S. Xiao and Y. Li, "Modeling and high dynamic compensating the rate-dependent hysteresis of piezoelectric actuators via a novel modified inverse Preisach model," IEEE Trans. Contr. Syst. Tech., vol.21, no.5, pp.1549-1557, 2013.

[24] F. Lin, S. Lee and P. Chou, "Intelligent nonsingular terminal sliding-mode control using MIMO elman neural network for piezo-flexural nanopositioning stage," IEEE Trans. Ultras., Ferroelec. Freq. Contr., vol.59, no.12, pp.2716-2730, 2012.